Materials Chemistry and Physics 128 (2011) 243–249

Contents lists available at ScienceDirect

Materials Chemistry and Physics

journal homepage: www.elsevier.com/locate/matchemphys

Controlled size formation of electrodeposited Pt–Ru nanostructured catalysts using chelating compounds

J.M. Sieben *,[1]

Instituto de Ingeniería Electroquímica y Corrosión (INIEC), Universidad Nacional del Sur, Av. Alem 1253, B8000CPB Bahía Blanca, Argentina

ARTICLE INFO

Article history:
Received 11 December 2009
Received in revised form 22 February 2011
Accepted 2 March 2011

Keywords:
Pt–Ru catalysts
Electrodeposition
Sodium citrate
Sodium tartrate
Na_2H_2EDTA
Methanol oxidation

ABSTRACT

The electrodeposition of Pt and Ru on a oxidized graphite cloth from H_2PtCl_6 and $RuCl_3$ solution containing trisodium citrate (Cit), disodium tartrate (Tar) and disodium dihydrogen ethylenediaminetetraacetate (Na_2H_2EDTA) as complexants was investigated. SEM image of the electrode prepared without complexant showed a continuous compact and rough deposit that covers the entire graphite fibers surface displaying the structure of a coating film, whereas particles with uniform size and globular shape regularly distributed over the support were obtained when the complexants were added to the solution. Thus, EDX and XRD analysis revealed changes in Pt–Ru catalyst composition. It was concluded from electrocatalytic activity measurements that the electrodes prepared using chelating compounds exhibited better CO tolerance and performance for methanol oxidation than that without complexant.

1. Introduction

Anodes for methanol oxidation in DMFC are porous electrodes constituted by a carbon substrate over which a bimetallic Pt–Ru electrocatalyst is distributed in form nanosized particles. It is well known that the oxidative removal of CO_{ads} by adsorbed oxygen containing species plays a dominant role in the determination of the catalyst activity for methanol oxidation. Pt–Ru solid solutions with low ruthenium content are recognized as the best catalysts for methanol oxidation in acid solutions at room temperature [1,2]. The higher activity of these bimetallic materials compared to pure Pt is generally explained by the bifunctional reaction mechanism [3–5]. According to this mechanism, the ruthenium centers are responsible for generation of active oxygen species, while platinum centers keep the adsorbed methanol species; that is, methanol oxidation proceed with the adsorption of methanol on Pt assembles and the oxidation of CO_{ads} by OH_{ads} adsorbed on Ru atoms.

The catalytic activity of supported systems essentially depends on the dispersion of the active component onto the inert support. The effective utilization of supported metallic particles can be achieved only if metal particles are well dispersed on the support with an adequate shape, size and roughness [6,7]. In addition, Gasteiger and Marković [8] have recently indicated that viable Pt-based catalysts, that is, with a high mass activity, must have a large particle dispersion and high turnover frequency (which quantifies the number of electrons produced per active site per second at a defined operating condition).

The development of supported Pt–Ru catalysts prepared by electrochemical procedures has received great attention during the last years, since the electrochemical techniques offer an effective way to deposit platinum and ruthenium selectively at desired locations on the electrode with both ionic and electronic access [9].

The production of catalyst nanoparticles by electrochemical techniques is very advantageous because the crucial steps in nanoparticles formation can be controlled by the adequate election of current density, and the use of complexing agents and grain refiners [10,11]. The current density or the overpotential is responsible for the number and size of nuclei. The use of organic additives enables the control of the crystallization process. Additionally, surface activation of carbon substrates produces surface groups that act as attachment centers for metallic particles.

Strong complexing agents such EDTA, citrate, and tartrate have been utilized in remediation of heavy metal contaminated soils [12], metal plating, water softening, photography, textile, paper manufacturing and industrial cleaning [13,14]. In catalyst synthesis the complexing agents have been habitually used to prevent the agglomeration of nano-sized catalyst particles, e.g. polyvinyl pirrolydone interact with Pt–Ru catalyst surface sites [15], while EDTA, tartaric acid and citric acid have been used as growth inhibitors in silver [16], nickel–tungsten alloy [17,18], tin–zinc alloy [19], and copper electrodeposition [20].

In this work, supported Pt–Ru nanostructured catalysts are prepared by electrodeposition in the presence of different com-

* Tel.: +54 291 4595182; fax: +54 291 4595182.
E-mail addresses: jmsieben@uns.edu.ar, jmsieben@yahoo.com.ar
[1] Comisión de Investigaciones Científicas de la Provincia de Buenos Aires (CIC).

0254-0584/$ – see front matter © 2011 Elsevier B.V. All rights reserved.
doi:10.1016/j.matchemphys.2011.03.006

plexants. The effect of Cit, Tar, and Na_2H_2EDTA on the particle size, morphology and active surface area is discussed. Moreover, the activity of these electrodes for methanol oxidation is evaluated.

2. Experimental

Graphite cloth (GC-10, from The Electrosynthesis Co., Inc.) of 1 cm^2 exposed geometric area was used as catalyst support. Electrochemical measurements were carried out in a conventional glass cell at room temperature after deaeration with nitrogen. A saturated calomel electrode and a Pt foil were used as the reference electrode and the counter electrode, respectively. All potentials mentioned in this work are referred to the calomel electrode (SCE), except for the cyclic voltammograms of methanol oxidation, where SHE scale was applied. A PAR 273A potentiostat was used to perform the electrochemical experiments. In addition, polish to mirror glassy carbon (GC) material of 0.07 cm^2 exposed geometric area was used as support to collect information about the catalyst structure and morphology using AFM microscopy.

Before the electrochemical deposition of the catalyst took place, the carbon supports were treated by anodic potentiostatic polarization in 0.5 M H_2SO_4 at 2 V for 60 s followed by a linear cathodic potential sweep down to −0.8 V (scan rate 1 mV s^{-1}) [21].

The catalysts were synthesized by electrodeposition at room temperature using a diluted solution of platinum and ruthenium salts (2 mM H_2PtCl_6 + 2 mM $RuCl_3$ in 0.5 M H_2SO_4) in combination with a chelating agent (0.02 M Cit, 0.02 M Tar, and 0.02 M Na_2H_2EDTA). The solution pH was adjusted to 3.5 with 1.0 M NaOH. Analytical grade reagents H_2PtCl_6 and $RuCl_3$ (40% w de Pt, 41% w de Ru from Fluka®), H_2SO_4 (96%, w/w from CarloErba®), $Na_3C_7H_5O_7$ (99.9% from Pa Alcor®), $Na_2C_4H_4O_6{\cdot}2H_2O$ (99.9% from Malinckrodt®), Na_2H_2EDTA (99.9% from ELL Lowens®), and bidistilled water were used. No attempt was made to control the pH during deposition, but pH was measured and, if necessary, adjusted, after each deposition experiment.

The electrodeposition was carried out potentiostatically at −0.5 V for 15 min. After deposition, the electrodes were thoroughly rinsed with bidistilled water and then tested in sulphuric acid solution. A lineal potential sweep from −0.25 V to 0.5 V was applied at a rate of 50 mV s^{-1}.

Cyclic voltammetry and chronoamperometry techniques were used to evaluate the performance of the electrodes in 1 M CH_3OH (99.9% from J.T. Baker®) + 0.5 M H_2SO_4 solution.

The active surface area of the electrocatalysts was determined by underpotential deposition of copper (Cu-UPD) [22]. First reference voltammograms were obtained in 0.1 M H_2SO_4 cycling between −0.25 V and 0.8 V at a scan rate of 10 mV s^{-1}. The electrodes were polarized at 0 V for 300 s to reduce the RuO_x formed during the cyclic voltammetry. The Cu-UPD experiments were carried out in 0.1 M H_2SO_4 and 2 mM $CuSO_4$ (99% from Merk®) solution. The working electrodes were polarized at 0.059 V for 300 s to form a monolayer of copper on the catalyst surface. A linear voltammetric scan with a scan rate of 10 mV s^{-1} was then performed between 0.059 V to 0.8 V to remove the adsorbed copper monolayer. The charges obtained for the copper stripping were corrected for the charges associated with background processes and oxide growth by subtracting the charge obtained from the reference scan in the same potential range. The integration of the peak area corresponding to the Cu-UPD stripping was used to determine the electroactive surface area, with the assumption of an adsorption ratio of a single Cu atom to each surface metal atom and a monolayer charge of 420 μC cm^{-2} [23]. Current densities for methanol oxidation are referred to the active surface area of the catalysts.

UV–vis spectrophotometry (Agilent 8453) was applied to characterize the metal ion solution in presence of different chelating compounds, using samples diluted in a rate 1:50 but maintaining the solution pH at a value of 3.5. The morphology and particle size of the catalyst were examined using scanning electronic microscopy (SEM, EVO 40 LEO) and non-contact atomic force microscopy (AFM, Nanoscope Digitals Instruments), and thus, particle size distribution analysis was carried out using ImageJ program. The structure of the electrodes was characterized by X-ray diffraction using a XRD, Rigaku Dmax III C diffractometer with a monochromated CuKα source operated at 40 keV at a scan rate of 0.05° s^{-1}. Bulk composition of Pt–Ru catalysts was performed using EDX analysis.

The amount of Pt and Ru deposited on the graphite cloth was estimated using an ICP-AES (Shimadzu 1000 model III). The samples were prepared by digesting the electrodes in boiling aqua regia and then removing excess acid. The catalyst loading was expressed in mg per unit of geometric area.

3. Results and discussion

Fig. 1 shows the UV–vis spectral change when the chelating compounds were added to the solution. In the solution without complexant there were two absorbance peaks at ∼200 and ∼260 nm, characteristic of $PtCl_4^{2-}$ and $PtCl_6^{2-}$, respectively [24–26]. The peak at 260 nm is the result of the ligand-to-metal charge transfer transition in the $PtCl_6^{2-}$ ions [26]. However, the characteristic Ru^{3+} ions or the ruthenium hydroxide complexes

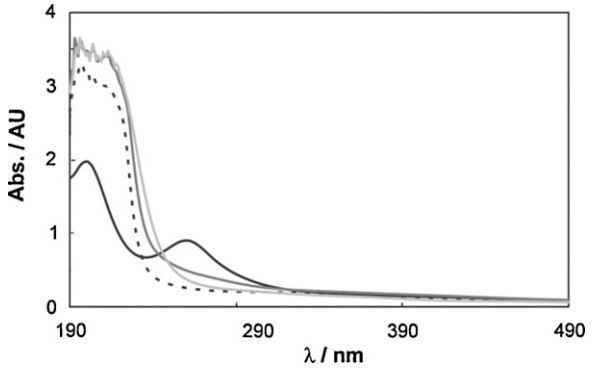

Fig. 1. UV–vis absorption spectra of solutions containing H_2PtCl_6 and $RuCl_3$ at room temperature. Without complexant (▬), Cit (▬), Tar (▬ ▬), and Na_2H_2EDTA (▬). The spectra were carried out using the electrodeposition solutions diluted in a rate 1:50 at pH 3.5.

absorption at 240 nm was absent or masked by the H_2PtCl_6 absorption at this wavelength [27]. The characteristic absorbance band at ∼260 nm disappeared upon the addition of Cit, Tar and Na_2H_2EDTA, but a wide absorbance band between 203 and 210 nm was observed. The appearance of this band may be related to the formation of chelate complexes with the polydentate ligand (Cit, Tar and Na_2H_2EDTA) by displacement of the chloride ion in $PtCl_6^{2-}$ [28,29]. In the presence of $HCit^{2-}$ (pK_{a2} = 4.37), Tar^{2-} (pK_{a2} = 4.34) and H_2EDTA^{-2} (pK_{a4} = 2.66), it is proposed that citrate, tartrate and EDTA complexation of Pt(IV) and Ru(III) would be formed to realize the stabilizing effect.

Fig. 2 shows linear sweep voltammetry curves recorded at GC-10 substrate in H_2SO_4 solution containing H_2PtCl_6 and $RuCl_3$ with and without the chelating agents respectively. The cathodic limit for the experiments was selected to be −0.3 V and −0.5 V, just negative to the potential where H_2 evolution beginning on the Pt–Ru particles formed during the deposition process. The curve corresponding to Pt and Ru deposition without complexant shows that Pt reduction begins at about 0.3 V and the current due to the reaction increases when the potential shifts to more negative values, becoming a mass transport controlled process [30]. In addition, it can be seen the presence of three overlapping reduction waves with half wave potentials at 0.13 V, −0.07 V and −0.18 V. Besides, the last wave is probably coupled with H^+ ion discharge on Pt nuclei. Pletcher and co-workers [31] believe that these loops can be fully explained by slow nucleation of Pt centers, where the solution contains substantial amount of $PtCl_6^{2-}$ and two species resulting from the hydrolysis reaction ($PtCl_5(H_2O)^-$ and $PtCl_4(H_2O)_2$), where each species is reduced to Pt(0). This interpretation coincides with the multiple cathodic waves observed in the figure, although the presence of Pt(+II) as a stable intermediate cannot be discarded.

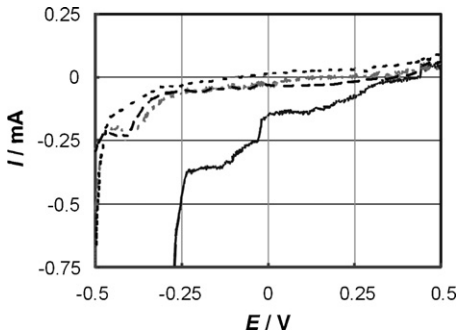

Fig. 2. Voltammetric curves for a GC-10 support in 2 mM H_2PtCl_6 + 2 mM $RuCl_3$ and 0.5 M H_2SO_4. Without complexant (▬), Cit (▬ ▮ ▬), Tar (▬ ▬), and Na_2H_2EDTA (▬ ▬ ▬). Scan rate 0.5 mV s^{-1}.

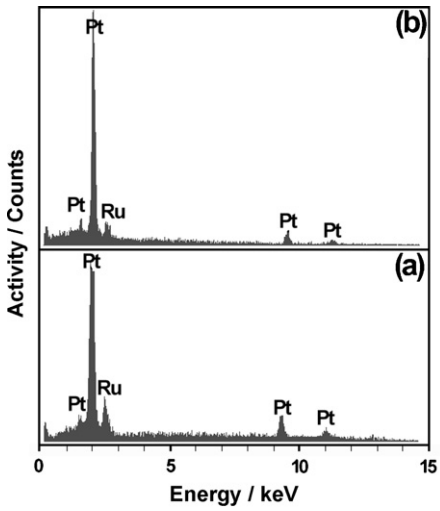

Fig. 3. EDX spectra of Pt–Ru/GC-10 electrodes. Without complexant (a), and Na_2H_2EDTA (b).

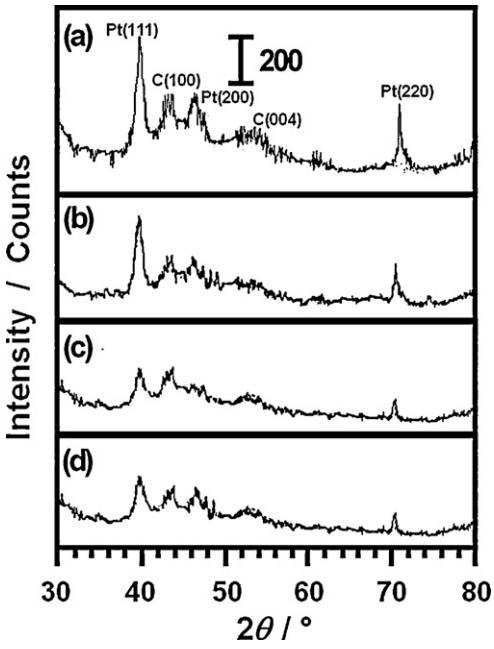

Fig. 4. XRD patterns of Pt–Ru/GC-10 electrodes. Without complexant (a), Cit (b), Tar (c), and Na_2H_2EDTA (d).

In addition, Ru deposition from $RuCl_5(H_2O)^{2-}$ ion could begin in the potential zone where $PtCl_5(H_2O)^-$ specie is reduced. It is known that the overpotential of Ru electrodeposition is rather high on carbon, but it is much lower on Pt, so Ru can be codeposited with Pt on carbon at a lower overpotential favored kinetically by Pt nuclei formed over the carbon support [32].

The organic compounds shifted Pt(+IV) reduction process towards more negative potentials. Indeed the electrodeposition of Pt appears to begin at about 0 V, and two reduction waves are only visible. This behavior can be connected to the existence of new species in the solution, i.e. carboxyl anion and amine groups act as a ligand forming chelate-type complexes with platinum and ruthenium ions. In addition, a significant reduction in the electrodeposition current is observed, which may represent inhibition of the deposition process. The decrease in current may be related to specific adsorption of the organic molecules over the metallic particles thus hindering electrodeposition [10,28,33–35].

The atomic compositions of Pt–Ru/GC electrodes were determined by EDX technique (Fig. 3) and ICP-AES analysis. The information of all catalysts from both analytical techniques is listed in Table 1.The ruthenium content of the catalyst prepared without complexant was about 25 at.%, whereas near 16 at.% was determined in those prepared with the chelating compounds (Table 1). The composition of the electrodeposits is known to mainly depend on bath composition and applied current density. The decrease in Ru content upon the addition of complexants may be due to additive adsorption on the cathode surface, limiting Ru^{3+} discharge. Moreover, the kinetic of Pt nucleation process may be decelerated, limiting Ru nucleation. Thus, differences in the stability constant of Ru and Pt ion complexes could explain this behavior. However, it is not clear, at the moment, which is the reason for this comportment; and this will be subject of further studies. The EDX spectra of the bimetallic catalysts and the corresponding XRD patterns (Fig. 4) do not show the presence of oxygen in the deposit.

The XRD patterns of the carbon supported Pt–Ru catalysts are shown in Fig. 4. The diffraction peaks referred to carbon support are located at 2θ values of about 43° and 54° in the XRD diffractograms. Moreover, three peaks characteristic of face centered cubic (fcc) crystalline at approximately 2θ values of 40°, 47° and 70°, which are associated with the (1 1 1), (2 0 0) and (2 2 0) planes respectively are observed, indicating that the catalysts have principally single-phase disordered structure (i.e., solid solution). It can be noted from the figure that all the diffraction peaks of Pt–Ru catalysts are slightly shifted to higher 2θ with respect to those of pure Pt (not shown), revealing the formation of an alloy involving the incorporation of Ru atoms into the fcc structure of Pt. It is important to note that no diffraction peaks indicating the presence of either pure Ru or Ru-rich hexagonal close packed (hcp) phase are observed, but their presence cannot be discarded because they may be present in a very small amount of metallic ruthenium and its oxides in the amorphous state forming clusters over the surface of the bimetallic particles.

The peak profiles in XRD patterns are obtained by integration of the respective areas after peak deconvolution using the Marquardt algorithm. A lattice parameter of 3.922 ± 0.002 Å is determined for Pt/GC-10 (not shown), which is in good agreement with pure

Table 1
Parameters of nanostructured Pt–Ru supported on oxidized graphite cloth.

Pt–Ru/GC-10	$X_{Ru(EDX)}$ (±0.05)	$X_{Ru(XRD)}$ (±0.08)	$d_{p(SEM)}$[a] (±10) nm	$d_{c(XRD)}$[b] (±2) nm	w_{Pt-Ru}[c] (±0.05) mg cm^{-2}	Pt:Ru[d] atomic ratio	S[e] (±1.3) cm^2	S_w (±0.9) m^2 g^{-1}
Without complexant	0.25	0.23	150	30	0.69	1:0.30	60.4	8.8
Cit	0.14	0.16	50	5	0.33	1:0.14	84.9	26.1
Tar	0.15	0.17	70	6	0.41	1:0.18	79.8	19.4
Na_2H_2EDTA	0.13	0.14	20	4	0.23	1:0.12	99.7	42.6

[a] d_p: particle size determined from SEM images.
[b] d_c: crystallite size determined from Debye–Scherrer's equation.
[c] w_{Pt-Ru}: catalyst loading measured using ICP-AES experiments.
[d] Pt:Ru atomic ratios calculated by ICP-AES results.
[e] Active surface area measured by Cu-UPD stripping.

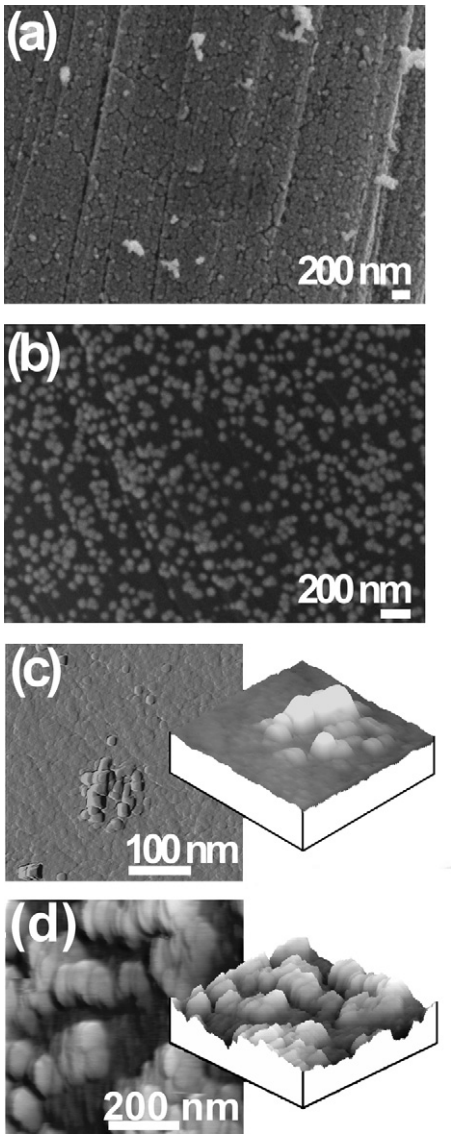

Fig. 5. Top-view SEM images of Pt–Ru/GC-10 electrodes without complexant (a), and Na_2H_2EDTA (b). Top-view and 3D AFM image of a Pt–Ru/GC electrode prepared using Na_2H_2EDTA as complexant (c).

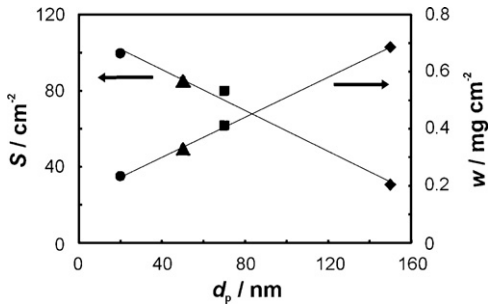

Fig. 6. Dependency of the active surface area S and catalyst mass per unit of geometric area w with the particle size for supported Pt–Ru catalysts. Without complexant (♦), Cit (▲), Tar (■), and Na_2H_2EDTA (●).

Pt (3.923 Å); whereas values of 3.895 ± 0.003 Å, 3.901 ± 0.004 Å, 3.903 ± 0.002 Å, and 3.902 ± 0.002 Å are measured in the bimetallic catalysts prepared without complexant, Cit, Tar and Na_2H_2EDTA respectively. In accordance with the Vegards' law, the nominal Ru content of the Pt–Ru catalyst agrees with EDX results (Table 1).

Debye–Scherrer's equation is used to estimate the average Pt–Ru crystallite size from Pt (1 1 1) and (2 2 0) peaks. When the catalyst is prepared from complex solutions the average size of the crystallites estimated by XRD is around 4–6 nm, whereas the mean crystallite size is 30 nm when there is no complexing agent. In addition, the ratio between (1 1 1) and (2 2 0) areas does not change significantly in these samples indicating the absence of preferential orientation.

Fig. 5(a) shows a SEM micrograph of Pt–Ru/GC-10 electrode prepared using the solution without complexant. The reduction process creates a rough coating film of Pt–Ru particles formed by several layers of globular particle agglomerates with sizes between 150 and 200 nm (Table 1), which follows the graphite cloths relief. This is the consequence of a higher number of nucleation sites on GC-10 support formed during the cathodic pulses. In addition, over the compact deposit some islands with incipient dendrites can be seen. Dendrite formation happens when a deposition process occurs in the mass-transfer or mixed control region [35]. In this condition, the dendrite growth is accelerated due to a faster diffusion rate of the metal ions at the tip of the excrescences [36].

The addition of Cit, Tar and Na_2H_2EDTA to the deposition bath (Fig. 5(b)) inhibits the formation of the coating film and the dendritic particles observed in Fig. 5(a). As a result, Pt–Ru particles exhibit uniform size and globular shape appearing regularly distributed over the support surface with sizes between 50 and 90 nm for Cit and Tar, and between 20 and 30 nm for Na_2H_2EDTA.

To obtain additional information by AFM microscopy planar Pt–Ru electrodes were prepared using GC as support. When complexants are used, i.e. Na_2H_2EDTA (Fig. 5(c)), metallic agglomerates constituted by nano-sized particles connected via intergrain boundaries are observed; whereas larger agglomerates constituted by bigger particles are observed in the sample without complexant (Fig. 5(d)). The mean particle size of the catalysts determined by AFM is in agreement with those determined from SEM images.

Comparing XRD and SEM it is concluded that Pt–Ru particles observed by SEM are, in fact, agglomerates comprised of nano-sized particles. Similar particle morphology was observed by Coutanceau et al. [37] on carbon-supported Pt–Ru/C catalysts prepared by galvanostatic pulse electrodeposition. It is known that electrodeposition of noble metals on carbon supports occurs via 3D nucleation and growth mechanism [38,39]. Generally, primary nucleation on carbon is followed by secondary nucleation on predeposited Pt surface, due to a higher concentration of nucleation centers on Pt surface compared to carbon. The result of secondary nucleation is the formation of complex micro and nano multi-grained Pt structures [40].

From Table 1 and Fig. 6 it can be seen that the active surface area, S, the catalyst loading, w, and the true surface area, S_w, are significant affected when the additives were added to the solution. The average size of Pt–Ru particles decreases with an increase in S and S_w, whereas, for the catalyst loading the inverse dependence is observed. The largest value of S_w is obtained with Na_2H_2EDTA addition, followed by Cit and Tar respectively. This result can be related to the decrease in Pt–Ru particle size and a remarkably uniform and high dispersion of the alloy particles, along with the reduction of Pt–Ru catalyst loading. The addition of the complexants results in a significant loading reduction for both metals following the order: Na_2H_2EDTA > Cit > Tar > without complexant. In the meantime, Ru mass loading is reduced more than that of Pt probably due to a kinetic reason. As was mentioned previously, the capacity of the organic agents to complex the metal ions, and the specific adsorption of these organic molecules inhibits particle growth and prevents particle agglomeration.

The first aspect is associated with the existence of species such as carboxyl anion and amines groups that can form chelate-type com-

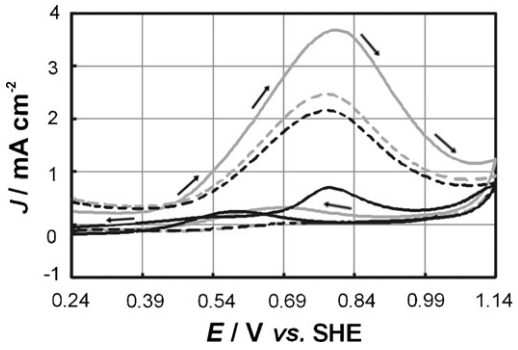

Fig. 7. Cyclic voltammograms of Pt–Ru/GC-10 electrodes in 1 M CH_3OH/0.5 M H_2SO_4. Without stabilizer (▬), Cit (▬ ▬), Tar (■ ■), and Na_2H_2EDTA (▬). Scan rate 50 mV s^{-1}. Potentials are expressed with respect to SHE scale.

plexes with platinum and ruthenium ions. On the other hand, the organic molecules in excess adsorb on the surface, blocking metal ions deposition and crystal growth. The tendency of the complexants to segregate towards the surface is favored by its polar nature, as was observed for the system nano-copper/citric acid [11], nano-nickel/saccharin [34], and nano-silver/EDTA [28]. The free electron pairs of the oxygen atoms in organic molecules can interact strongly with Pt–Ru particles being attracted to the electrode due to the presence of a strong electric field allowing larger surface energy of the whole system as was suggested by Shimazaki et al. [41]. On the other hand, the differences observed between Cit, Tar and Na_2H_2EDTA can be linked to differences in the stability of Pt(+IV) and Ru(+III) ion complexes formed after the addition of the organic compounds.

Fig. 7 shows the cyclic voltammograms recorded at 50 mV s^{-1} in 1 M CH_3OH + 0.5 M H_2SO_4 solution at room temperature. For all the electrodes the onset of the methanol oxidation reaction takes place near 0.2 V. The beginning of methanol electro-oxidation at this potential can be associated with the formation of OH_{ads} species on Ru atoms originating in the water dissociation that occurs at potentials more negative than that on Pt atoms, through the so called bifunctional mechanism [42,43] such as shown below. At room temperature, CH_3OH is adsorbed only on Pt sites, while water molecules dissociates on Ru giving OH_{ads} (step 3) and the species adsorbed on Pt and Ru combine together forming CO_2 (step 4) in a Langmuir–Hinshelwood (L–H) type reaction [3].

$$CH_3OH + Pt \rightarrow Pt\text{–}CH_3OH_{ads} \quad (1)$$

$$Pt\text{–}CH_3OH_{ads} \rightarrow Pt\text{–}CO_{ads} + 4H^+ + 4e^- \quad (2)$$

$$H_2O + Ru \rightarrow Ru\text{–}OH_{ads} + H^+ + e^- \quad (3)$$

$$Pt\text{–}CO_{ads} + Ru\text{–}OH_{ads} \rightarrow Pt + Ru + CO_2 + H^+ + e^- \quad (4)$$

A methanol oxidation peak during the forward scan at about 0.55 V and another anodic peak on the reverse scan, ca. 0.33 V, due to the removal of incompletely oxidized species, i.e. CO, formed in the forward scan can be seen. The potentiodynamic measurements suggests that Pt–Ru/GC-10 catalyst prepared using Na_2H_2EDTA as complexant presents the greatest activity for methanol oxidation, followed by those prepared using Cit and Tar.

The performance of the bimetallic catalysts for methanol oxidation is compared using the ratio of current densities associated with the anodic peaks in the forward (J_{pf}) and reverse (J_{pb}) scans. This relationship has been used to infer the CO tolerance of the catalyst [44]. A lower J_{pf}/J_{pb} value indicates a poor oxidation of methanol during the anodic scan and excessive accumulation of carbonaceous species on the catalyst surface [45]. Therefore, a higher J_{pf}/J_{pb} value is indicative of improved CO tolerance. It can be seen that the electrodes prepared using the chelating compounds display

Table 2
Catalytic activity of supported Pt–Ru/GC-10 electrodes.

Solution	J[a] mA cm^{-2}		J_w[b] A g^{-1}		J_{pf}/J_{pb}
	0.2 V	0.3 V	0.2 V	0.3 V	
–	0.02	0.06	1.8	5.3	2.8
Cit	0.18	0.40	47.0	104.5	18.1
Tar	0.13	0.23	25.2	44.7	16.7
H_2EDTA	0.39	0.82	166.1	349.4	12.0

[a] J: current density per unit of active surface area.
[b] J_w: current density per unit mass of catalyst.

the best CO resistance among the prepared catalysts (Table 2). This behavior could be related to the presence of high intergrain boundaries, providing active sites for water adsorption and dissociation and, thus for the oxidation of CO and methanol [40].

In a parallel work, current transient measurements at constant potentials were carried out for 600 s (Fig. 8), showing that the different electrodes present the same behavior as that observed in the voltammetric curves. The results are summarized in Table 2. Chronoamperometric curves in Fig. 8 shows a high initial current density for methanol oxidation, which rapidly decays to a much lower value. This current decay is observed in the literature for bimetallic Pt–Ru catalysts at diverse temperatures and methanol concentrations [4,43]. Gasteiger et al. [43] indicated that deactivation is caused by blocking access of the active sites due to the formation of poisoning species. Chemisorption of methanol gives rise to the adsorption of CHO and CO intermediaries with the former detected at short adsorption times and low potentials.

Electrocatalyst performance for methanol oxidation of the most active home-made supported Pt–Ru catalyst results highly competitive when it is compared with some chemical-synthesized catalysts reported in the literature (Table 3). The electrodes activity for methanol oxidation does not follow the order of decreasing particle size, from which home-made catalyst performance would be expected to be lower than those listed in Table 3. It is therefore necessary to reach a reasonable explanation that can satisfy this behavior.

The enhanced catalytic activity of the home-made electrode prepared using Na_2H_2EDTA as complexant may be associated with:

1. Catalyst-support interaction
2. Concentration of surface defects
3. Catalyst composition
4. Extent of catalyst surface oxidation

The presence of functional groups can contribute to improve electrode performance. Activation of carbon material increases its hydrophilicity, making the surface more accessible to the metal precursor. Under favorable wetting conditions electrostatic effects mainly determine the amount of Pt adsorbed by carbon in the

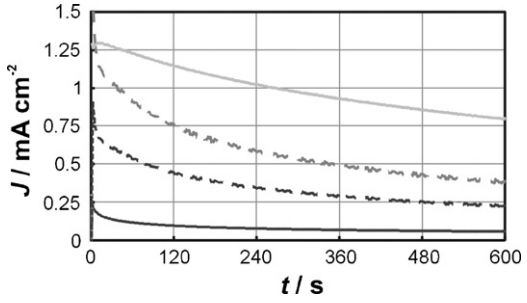

Fig. 8. Chronoamperometry curves at 0.3 V vs. SCE for Pt–Ru/GC-10 electrodes in 1 M CH_3OH/0.5 M H_2SO_4. Without stabilizer (▬), Cit (▬ ▬), Tar (■ ■), and Na_2H_2EDTA (▬).

Table 3
Quasi-stationary current densities at of methanol oxidation on supported Pt–Ru catalysts as synthesized in this work and prepared by other techniques.

Pt–Ru	X_{Ru}	$d_p$nm	w[a] mg cm^{-2}	S_w m^2 g^{-1}	JmA cm^{-2}	J_wA g^{-1}
This work	0.13	20	0.23	42.6	0.82	349.4
[46]	0.40	2.5	0.24	–	0.08	–
[47]	0.41	2.3	0.24	–	0.03	–
[48]	0.30	20	0.11	–	0.08	45.9
[49]	0.33	5.0	–	–	–	23
[50]	0.50	4.0	13.3	–	–	4.5
[51]	0.47	3.9	1.0	55.8	0.05	27.9
[52]	0.32	2.0	0.08	–	–	37.3
[53]	0.10	3.9	0.71	–	–	185.0
Commercial[b]	0.50	2–4	–	–	–	7–10

[a] w: catalyst mass per unit of geometric area.
[b] E-TEK® Pt–Ru/C (40 and 20 wt.%; Pt:Ru mol ratio 1:1) catalysts; data from Refs. [49,52].

equilibrium impregnation with an aqueous solution of hexachloroplatinic acid [54]. In other words, the oxygen-containing groups act as anchoring sites for catalyst particles or their precursors. In the former case, the precursor is supposed to distribute more uniformly over the carbon surface to provide a higher dispersion of metal and to make sintering more difficult (quantum chemical calculations and experimental observations indicate that heterogeneous surfaces can better stabilize metal in highly dispersed state) [55]. Carbon support influence the nature of catalyst particles due to electronic interactions as a result of collective interactions defined primarily by the bulk electronic structure of the two phases or as a result of the interaction of metal clusters with local sites of the support with specific properties such as acidity or basicity [56]. Therefore the electronic interactions could influence the size and morphology of metal crystallite, their surface and bulk properties, resistance to coalescence and poisoning. Therefore, the interactions at the metal-support interface can decrease the adsorption strength of methanolic residues [56]. Besides, the oxidized groups could facilitate the accessibility of methanol to the electroactive surface and participate in the oxidation of the absorbed intermediate species formed in alcohol dissociation.

Nanostructured catalysts habitually exhibit a large quantity of surface defects, and these defects substantially affect the catalyst behavior. It should be noted that the specific surface area estimated from XRD using Eq. (5) considerably exceeds the values observed in Table 1, i.e. S_w value of the catalyst prepared using Na_2H_2EDTA as complexant is 42.6 m^2 g^{-1}, while $S_{w,cal}$ value calculated from the results of XRD is 65.6 m^2 g^{-1}.

$$S_{w,cal} = \frac{6000}{\rho_{Pt-Ru} d_c} \quad (5)$$

where $S_{w,cal}$ and d_c are the specific surface area and the crystallite size respectively, determined from the results of XRD and ρ_{Pt-Ru} is the density of the alloy determined from catalyst composition.

This behavior can be explained by particle agglomeration at the experimental conditions used to prepare the catalysts. The degree of particle coalescence ξ can be calculated with Eq. (2) [57]:

$$\xi = 1 - \frac{S_w}{S_{w,cal}} \quad (6)$$

Here S_w is the specific surface area determined from Cu stripping and ICP analysis (Table 1). The calculation gives a ξ value of about 0.35, indicating some degree of particle agglomeration. ξ can be used as an indirect measured for the concentration of the grain boundaries regions, so the concentration of grain boundaries should be high. In this way, the home-made catalysts are formed by agglomerates composed of nano-sized metal grains interconnected via grain boundaries, resulting in the formation of multi-grained structures. According to the recent molecular-dynamics simulations of the structure and deformation behavior of nano-crystalline materials performed by Wolf et al. [58], nanostructured materials may be represented as consisting of highly ordered crystalline domains surrounded by disordered region of about 0.5 nm wide. These discontinuities in the crystal planes may act similarly to low coordinated sites (steps and kinks) on single crystalline and other extended surfaces [57], which exhibit very high catalytic activity for methanol oxidation. Metal atoms on proximity of grain boundaries usually have decreased number of neighbors in the first coordination shell, and thus, are expected to bind adsorbates and catalyze bond-breaking reactions like methanol dissociative chemisorption [59].

On the other hand, the catalysts prepared by chemical techniques usually exhibits particle sizes between 2 and 5 nm. A low activity of small particles in methanol oxidation has been noticed by Takasu et al. [60] and was attributed to the 'negative' particle size effect; since small Pt–Ru particles are more susceptible to CO poisoning. This observation is supported by the evidence presented by Mukerjee and McBreen [61]. In this investigation smaller particles (<5 nm) with their higher proportion of low coordination sites (greater number of surface sites with higher Pt d-band vacancies) adsorbs species such as H, OH and CO more strongly.

Moreover, some differences in the catalytic performance of the electrodes can be attributed to changes in the alloy composition. In general, surface reactions require a specific geometric orientation and a suitable atomic configuration at the surface allowing the reactants to be in an appropriate binding situation. The lower Ru content on the Pt–Ru/GC-10 electrode probably has some positive effect on the catalyst activity at room temperature. When Ru content exceeds 20 at.% the surface sites available to methanol adsorption decrease reducing the activity of the catalyst. This result can be easily explained assuming a random distribution of Pt and Ru in the surface as was recently outlined by Hoster et al. [62]. This behavior can be understood by some geometrical considerations, i.e. the perimeter of Ru islands on the Pt(1 1 1) surface influence the activity for methanol oxidation. Hoster et al. [62] observed that the activity for methanol starts to decrease as soon as alcohol adsorption at the free Pt sites is hindered by too-high Ru coverage. Thus, they emphasizes the importance of low-coordinated Ru sites at edge positions for the performance of the bifunctional mechanism at Pt(1 1 1)–Ru surfaces. These results may be extended to explain the behavior of supported Pt–Ru nanostructured catalysts.

Finally, another reason that can be put forward to explain the lesser activity of the catalysts synthesized by chemical methods may be related to the nature of Pt–Ru species in the catalyst surface. Analysis of the catalysts by photoelectron spectroscopy are conclusive on the presence of Pt, Pt(II) and Pt(IV) species in most of the catalysts prepared by chemical methods [47]. The presence of oxidized Pt species such as PtO and PtO_2 in these Pt–Ru supported catalysts would contribute to their lesser activity due to a reduction of the available sites for methanol adsorption. Raman et al. [63] found that the reduced nanoparticles were more active towards methanol oxidation than the fully or partially oxidized.

4. Conclusions

The addition of complexants to the deposition bath controls the structural characteristics of the electrodeposits. The behavior of the bimetallic electrodes can be associated with the catalyst particle size and particularly agglomerate size, true surface area, and composition of the deposit.

The most active electrocatalyst for methanol oxidation was prepared using Na_2H_2EDTA as complexant followed by the electrode prepared using Cit and Tar. The results can be explained considering that the complexes formed with Na_2H_2EDTA are more stable than those formed with Cit and Tar, exerting an important influence on the electrodeposition kinetics of the metals. In addition, the specific adsorption of organic molecules can contribute to the inhibition of particle growth.

From a practical point of view the electrode prepared with Na_2H_2EDTA appears to be interesting as materials for applications, and not as exclusively model systems, since it combines a good intrinsic activity and a high true surface area with low catalyst loading that make it possible to obtain good catalytic activity for methanol oxidation.

Acknowledgements

The author thanks CONICET, ANPCYT, CIC and SECyT UNS, Argentina. J.M.S. wishes to thank Dr. G. Mas for her assistance in the XRD measurements.

Appendix A. Supplementary data

Supplementary data associated with this article can be found, in the online version, at doi:10.1016/j.matchemphys.2011.03.006.

References

[1] T. Iwasita, in: W. Vielstich, et al. (Eds.), Handbook of Fuel Cells – Fundamentals, Technology and Applications, vol. 2, John Wiley & Sons, New York, 2003.
[2] P. Strasser, in: W. Vielstich, et al. (Eds.), Handbook of Fuel cells – Fundamentals, Technology and Applications, vol. 5, John Wiley & Sons, New York, 2009, pp. 30–47 (Chapter 3).
[3] M. Watanabe, S. Motoo, J. Electroanal. Chem. 60 (1975) 267–273.
[4] H.A. Gasteiger, N.M. Marković, P.N. Ross Jr., E.J. Cairns, J. Phys. Chem. 97 (1993) 12020–12029.
[5] V. Di Noto, E. Negro, R. Gliubizzi, S. Lavina, G. Pace, S. Gross, C. Maccato, Adv. Funct. Mater. 17 (2007) 3626–3638.
[6] T. Frelink, W. Visscher, J.A.R. van Veen, J. Electroanal. Chem. 382 (1995) 65–72.
[7] T.S. Ahmadi, Z.L. Wang, T.C. Grean, A. Henglein, M.A. El-Sayed, Science 273 (1996) 1924–1925.
[8] H.A. Gasteiger, N.M. Marković, Science 324 (2009) 48–49.
[9] C.R.K. Rao, D.C. Trivedi, Coord. Chem. Rev. 249 (2005) 613–631.
[10] H. Natter, R. Hempelmann, J. Phys. Chem. 100 (1996) 19525–19532.
[11] A.M. Alfantazi, U. Erb, J. Mater. Sci. Lett. 15 (1996) 1361–1363.
[12] R. Abumaizar, L.L. Khan, J. Air Waste Manage Assoc. 46 (1996) 765–774.
[13] M. Conway, S. Holoman, L. Jones, R. Leenhouts, G. Williamson, Chem. Eng. 106 (1999) 86–90.
[14] R.M. Spearot, J.V. Peck, Environ. Prog. 3 (1984) 124–128.
[15] A. Dalmia, C.L. Lineken, R.F. Savinell, J. Colloid Interface Sci. 205 (1998) 535–537.
[16] M.D. Obradović, R.M. Stevanović, A.R. Despić, J. Electroanal. Chem. 552 (2003) 185–196.
[17] O. Younes, L. Zhu, Y. Rosenberg, Y. Shacham-Diamand, E. Gileadi, Langmuir 17 (2001) 8270–8275.
[18] E. Guaus, J. Torrent-Burgués, J. Electroanal. Chem. 575 (2005) 301–305.
[19] G.M. Zarkadas, A. Stergiou, G. Papanastasiou, J. Appl. Electrochem. 34 (2001) 1251–1259.
[20] G.M. Zarkadas, A. Stergiou, G.G. Papanastasiou, Electrochim. Acta 50 (2005) 5022–5031.
[21] J.M. Sieben, M.M.E. Duarte, C.E. Mayer, ChemCatChem 2 (2010) 182–189.
[22] C.L. Green, A. Kucernak, J. Phys. Chem. B 106 (2002) 1036–1047.
[23] J.M. Sieben, M.M.E. Duarte, C.E. Mayer, J. Appl. Electrochem. 38 (2008) 483–490.
[24] J.F. Rivadulla, M.C. Vergara, M.C. Blanco, M.A. López-Quintela, J. Rivas, J. Phys. Chem. B 101 (1997) 8997–9004.
[25] A. Henglein, B.G. Ershov, M. Malow, J. Phys. Chem. 99 (1995) 14129–14136.
[26] T. Teranishi, M. Hosoe, T. Tanaka, M. Miyake, J. Phys. Chem. B 103 (1999) 3818–3827.
[27] V.I. Pârvulescu, S. Coman, P. Palade, D. Macovei, C.M. Teodorescu, G. Filoti, R. Molina, G. Poncelet, F.E. Wagner, Appl. Surf. Sci. 141 (1999) 164–176.
[28] J.C. Bailar Jr., The Chemistry of the Coordination Compound, Chapman & Hall, London, 1956.
[29] M. Gerloch, E.C. Constable, Transition Metal Chemistry, VHC, Weinheim, Germany, 1994.
[30] M.M.E. Duarte, A.S. Pilla, J.M. Sieben, C.E. Mayer, Electrochem. Commun. 8 (2006) 159–164.
[31] H.M. Yasin, G. Denuault, D. Pletcher, J. Electroanal. Chem. 633 (2009) 327–332.
[32] C. Bock, C. Paquet, M. Couillard, G.A. Botton, B.R. MacDougall, J. Am. Chem. Soc. 126 (2004) 8028–8037.
[33] H. Wang, Y. Zhao, Z. Jusys, R.J. Behm, J. Power Sources 155 (2006) 33–46.
[34] H. Natter, M. Schmelzer, R. Hempelmann, J. Mater. Res. 13 (1998) 1186–1197.
[35] J.O'M. Bockris, S.U.M. Khan, Surface Electrochemistry. A Molecular Level Approach, Plenum Press, New York, 1993, p. 361.
[36] A.J. Bard, C.R. Faulkner, Electrochemical Methods Fundamentals and Applications, 2nd edn., Wiley & Sons Inc., Singapore, 1980.
[37] C. Coutanceau, A.F. Rakotondrainibé, A. Lima, E. Garnier, S. Pronier, J.-M. Léger, C. Lamy, J. Appl. Electrochem. 34 (2004) 61–66.
[38] F. Gloaguen, J.-M. Léger, C. Lamy, A. Marmann, U. Stimming, R. Vogel, Electrochim. Acta 44 (1999) 1805–1816.
[39] J.V. Zoval, J. Lee, S. Gorer, R.M. Penner, J. Phys. Chem. B 102 (1998) 1166–1175.
[40] A.N. Gavrilov, E.R. Savinova, P.A. Simonov, V.I. Zaikovskii, S.V. Cherepanova, G.A. Tsirlina, V.N. Parmon, Phys. Chem. Chem. Phys. 9 (2007) 5476–5489.
[41] Y. Shimazaki, Y. Kobayashi, S. Yamada, T. Miwa, M. Konno, J. Colloid Interface Sci. 292 (2005) 122–126.
[42] V.S. Bagotzky, Y.B. Vassilyev, Electrochim. Acta 12 (1967) 1323–1343.
[43] H.A. Gasteiger, N. Markovic, P.N. Ross, E. Cairns, J. Electrochem. Soc. 141 (1994) 1795–1803.
[44] Z. Liu, X.Y. Ling, X. Su, J.Y. Lee, J. Phys. Chem. B 108 (2004) 8234–8240.
[45] T.C. Deivaraj, J.Y. Lee, J. Power Sources 142 (2005) 43–49.
[46] J.L. Gómez de la Fuente, M.V. Martínez-Huerta, S. Rojas, P. Terreros, J.L.G. Fierro, M.A. Peña, Carbon 43 (2005) 3002–3005.
[47] J.L. Gómez de la Fuente, M.V. Martínez-Huerta, S. Rojas, P. Terreros, J.L.G. Fierro, M.A. Peña, Catal. Today 116 (2006) 422–432.
[48] C. Bock, M.A. Blakely, B. MacDougall, Electrochim. Acta 50 (2005) 2401–2414.
[49] L.S. Sarma, T.D. Lin, Y.-W. Tsai, J.M. Chen, B.J. Hwang, J. Power Sources 139 (2005) 44–54.
[50] A.O. Neto, R.R. Dias, M.M. Tusi, M. Linardi, E.V. Spinacé, J. Power Sources 166 (2007) 87–91.
[51] T. Vidaković, M. Christov, K. Sundmacher, K.S. Nagabhushana, W. Fei, S. Kinge, H. Bönnemann, Electrochim. Acta 52 (2007) 2277–2284.
[52] P. Sivakumar, V. Tricoli, Electrochim. Acta 51 (2006) 1235–1243.
[53] Q. Lu, B. Yang, L. Zhuang, J. Lu, J. Phys. Chem. B 109 (2005) 1715–1722.
[54] M.A. Fraga, E. Jordão, M.J. Mendes, M.M.A. Freitas, J.L. Faria, J.L. Figueiredo, J. Catal. 209 (2002) 355–364.
[55] P.A. Simonov, V.A. Likholobov, in: A. Wieckowski, E.R. Savinova, C.G. Vayenas (Eds.), Catalysis and Electrocatalysis at Nanoparticle Surface, Marcel Dekker, New York, 2003 (Chapter 12).
[56] X.E. Verykios, in: A. Wieckowski, E.R. Savinova, C.G. Vayenas (Eds.), Catalysis and Electrocatalysis at Nanoparticle Surface, Marcel Dekker, New York, 2003 (Chapter 20).
[57] A.N. Gavrilov, E.R. Savinova, P.A. Simonov, V.I. Zaikovzkii, S.V. Cherepanova, G.A. Tsirlina, V.N. Parmon, Phys. Chem. Chem. Phys. 9 (2007) 5476–5489.
[58] D. Wolf, V. Yamakov, S.R. Phillpot, A. Mukherjee, H. Gleiter, Acta Mater. 53 (2005) 1–40.
[59] O.V. Cherstiouk, A.N. Gavrilov, L.M. Plyasova, I.Y. Molina, G.A. Tsirlina, E.R. Savinova, J. Solid State Electrochem. 12 (2008) 497–509.
[60] Y. Takasu, T. Fujiwara, Y. Murakami, K. Sasaki, M. Oguri, T. Asaki, W. Sugimoto, J. Electrochem. Soc. 147 (2000) 4421–4427.
[61] S. Mukerjee, J. McBreen, J. Electroanal. Chem. 448 (1998) 163–171.
[62] H.E. Hoster, A. Bergbreiter, P.M. Erne, T. Hager, H. Rauscher, R.J. Behm, Phys. Chem. Chem. Phys. 10 (2008) 3812–3823.
[63] R.K. Raman, A.K. Shukla, A. Gayena, M.S. Hegde, K.R. Priolkar, P.R. Sarode, S. Emura, J. Power Sources 157 (2006) 45–55.